Ablation of cardiac myosin–binding protein-C accelerates contractile kinetics in engineered cardiac tissue

Willem J. de Lange, Adrian C. Grimes, Laura F. Hegge, and J. Carter Ralphe

Department of Pediatrics, University of Wisconsin School of Medicine and Public Health, Madison, WI 53792

Hypertrophic cardiomyopathy (HCM) caused by mutations in cardiac myosin–binding protein-C (cMyBP-C) is a heterogenous disease in which the phenotypic presentation is influenced by genetic, environmental, and developmental factors. Though mouse models have been used extensively to study the contractile effects of cMyBP-C ablation, early postnatal hypertrophic and dilatory remodeling may overshadow primary contractile defects. The use of a murine engineered cardiac tissue (mECT) model of cMyBP-C ablation in the present study permits delineation of the primary contractile kinetic abnormalities in an intact tissue model under mechanical loading conditions in the absence of confounding remodeling events. We generated mechanically integrated mECT using isolated postnatal day 1 mouse cardiac cells from both wild-type (WT) and cMyBP-C–null hearts. After culturing for 1 wk to establish coordinated spontaneous contraction, we measured twitch force and Ca^{2+} transients at 37°C during pacing at 6 and 9 Hz, with and without dobutamine. Compared with WT, the cMyBP-C–null mECT demonstrated faster late contraction kinetics and significantly faster early relaxation kinetics with no difference in Ca^{2+} transient kinetics. Strikingly, the ability of cMyBP-C–null mECT to increase contractile kinetics in response to adrenergic stimulation and increased pacing frequency were severely impaired. We conclude that cMyBP-C ablation results in constitutively accelerated contractile kinetics with preserved peak force with minimal contractile kinetic reserve. These functional abnormalities precede the development of the hypertrophic phenotype and do not result from alterations in Ca^{2+} transient kinetics, suggesting that alterations in contractile velocity may serve as the primary functional trigger for the development of hypertrophy in this model of HCM. Our findings strongly support a mechanism in which cMyBP-C functions as a physiological brake on contraction by positioning myosin heads away from the thin filament, a constraint which is removed upon adrenergic stimulation or cMyBP-C ablation.

The Journal of General Physiology

INTRODUCTION

Cardiac myosin–binding protein-C (cMyBP-C) is an integral sarcomeric protein that is a major determinant of cardiac functional reserve (Davis et al., 2008). Mutations in cMyBP-C are a prevalent cause of hypertrophic cardiomyopathy (HCM) and sudden cardiac death in humans (Harris et al., 2011). The majority of HCM-causing mutations in cMyBP-C result in the truncation of the protein and are thought to cause HCM through haploinsufficiency (van Dijk et al., 2009; Carrier et al., 2010). Mouse models in which cMyBP-C is homozygously ablated (cMyBP-$C^{-/-}$) have been used extensively to study the role of cMyBP-C in normal cardiac contractility and the development of HCM (McConnell et al., 1999; Harris et al., 2002; Carrier et al., 2004). These models have provided invaluable insight into the role of cMyBP-C in the sarcomere and its involvement in the development of HCM. However, interpretation of results obtained from these models is confounded by the fact that hearts from cMyBP-$C^{-/-}$ mice undergo severe hypertrophic and dilatory remodeling during perinatal development (McConnell et al., 1999; Harris et al., 2002; de Lange et al., 2011), making it difficult to assess which contractile defects are caused by cMyBP-C ablation and which are the result of secondary remodeling.

cMyBP-C functions as a physiological "brake" on contractility that is relieved by phosphorylation upon β-adrenergic stimulation through activation of PKA. Upon phosphorylation by PKA (and/or other kinases), inhibitory interactions between cMyBP-C and other myofibril components are released (Gruen and Gautel, 1999; Gruen et al., 1999; Razumova et al., 2006; Shaffer et al., 2009; Barefield and Sadayappan, 2010; Kensler et al., 2011; Sadayappan et al., 2011), increasing the probability in myosin-actin cross-bridge formation (Weisberg and Winegrad, 1996). The net effect is predicted to lead to an increase in force production and accelerated contractile kinetics, which together contribute to the dynamic capacity of the heart to respond to increased demand for cardiac output. cMyBP-$C^{-/-}$ mice were used by several investigators to indirectly study the effect of PKA-mediated

Correspondence to J. Carter Ralphe: jcralphe@pediatrics.wisc.edu

Abbreviations used in this paper: CM, cardiomyocyte; DAPI, 4′,6-diamidino-2-phenylindole; HCM, hypertrophic cardiomyopathy; LV, left ventricular; mECT, murine engineered cardiac tissue.

The Rockefeller University Press $30.00
J. Gen. Physiol. Vol. 141 No. 1 73–84
www.jgp.org/cgi/doi/10.1085/jgp.201210837

phosphorylation of cMyBP-C, assuming that ablation should functionally mimic a fully phosphorylated cMyBP-C and abrogate its inhibitory effects upon contractility. Paradoxically, these studies have generally shown a decrease, rather than the predicted increase, in cardiac contractility (Harris et al., 2002; Carrier et al., 2004; Brickson et al., 2007; Tong et al., 2008). Although some studies showed acceleration in contractile kinetics (Harris et al., 2002; Korte et al., 2003; Stelzer et al., 2006a,b,c, 2007; Tong et al., 2008), others showed a deceleration (Carrier et al., 2004; Pohlmann et al., 2007). The divergence of findings from what might be predicted was most likely affected by the significant hypertrophic remodeling that occurs in cMyBP-C$^{-/-}$ hearts.

To better understand the primary contractile effects of cMyBP-C ablation in the absence of secondary remodeling, we developed a multicellular murine engineered cardiac tissue (mECT) system that uses neonatal cardiomyocytes (CMs) from cMyBP-C$^{-/-}$ mice that have yet to undergo hypertrophic remodeling (de Lange et al., 2011). Although hearts from cMyBP-C$^{-/-}$ mice undergo hypertrophy in the early perinatal phase, molecular markers of cardiac hypertrophy were absent in cMyBP-C$^{-/-}$ mECT (de Lange et al., 2011). Furthermore, in agreement with the hypothesized impact of cMyBP-C ablation detailed above, the initial characterization of the cMyBP-C$^{-/-}$ mECT model produced increased twitch force amplitude with faster contraction kinetics compared with WT control mECT (de Lange et al., 2011). These findings led us to hypothesize that the loss of cMyBP-C results in a constitutive increase in contractile velocity, rendering the myocardium unable to respond to lusitropic physiological stimuli such as β-adrenergic stimulation or increased heart rate. To test this hypothesis, we performed a detailed evaluation of the kinetic effects of cMyBP-C ablation in our prehypertrophic mECT model at physiological temperature with and without adrenergic stimulation and electrical pacing. Our data indicate that in the absence of cMyBP-C, cardiac contractile kinetics are near maximally accelerated and cannot further accelerate upon adrenergic stimulation or increased pacing frequency. This lack of kinetic reserve is independent of changes in Ca^{2+} transient kinetics, suggesting that cMyBP-C affects contractile kinetics through modulating cross-bridge cycling.

MATERIALS AND METHODS

Animals

Ventricular tissue was harvested from 1-d-old homozygous cMyBP-C$^{-/-}$ mouse pups that were previously generated on the E129X1/SvJ background (Harris et al., 2002) and from 1-d-old WT E129X1/SvJ mice (Taconic). Pups were anesthetized using inhaled isoflurane before harvesting of ventricular tissue. Additionally, 1- and 10-d-old WT and cMyBP-C$^{-/-}$ pups were used for echocardiographic measurements. This study was approved by the Animal Care and Use Committee of the School of Medicine and Public Health at the University of Wisconsin–Madison in accordance with the Guide for the Care and Use of Laboratory Animals (National Institutes of Health publication no. 85-23, revised 1985).

Isolation of neonatal mouse ventricular cardiac cells

Ventricular cardiac cells were isolated using enzymatic dissociation methods used to isolate neonatal mouse CMs as previously described (de Lange et al., 2011). In brief, excised ventricular tissue was minced and suspended in 3 mg/ml collagenase type II (Gibco) in KG buffer, pH 7.4, and incubated at 37°C for 20 min with gentle agitation. KG buffer consisted of 127 mmol/liter L-glutamic acid potassium salt monohydrate (Sigma-Aldrich), 0.1335% (wt/vol) $NaHCO_3$ (Gibco), 16.5 mmol/liter D-glucose (Sigma-Aldrich), 0.42 mmol/liter Na_2HPO_4 (Sigma-Aldrich), and 25 mmol/liter HEPES (Sigma-Aldrich). Ventricular tissue was subsequently suspended and agitated in 0.025% trypsin (Gibco) in KG buffer for 10-min intervals until dispersed. Cells were pelleted at 200 *g* and resuspended in mouse culture media consisting of 60.3% high-glucose DMEM (Gibco), 20% F12 nutrient mix (Gibco) supplemented with 1 mg/ml gentamicin (Sigma-Aldrich), 8.75% fetal bovine serum (HyClone), 6.25% horse serum (HyClone), 1% HEPES, 1× nonessential amino acid cocktail (Gibco), 3 mmol/liter sodium pyruvate (Gibco), 0.00384% (wt/vol) $NaHCO_3$, and 1 µg/ml insulin (Sigma-Aldrich). Cell suspensions were preplated onto P100 cell culture dishes and incubated at 37°C for 45 min to allow preferential attachment of nonmyocyte cell populations. Cardiac cells remaining in suspension were collected, checked for viability by dye exclusion, counted, and prepared for subsequent mECT construction.

mECT construction

WT and cMyBP-C$^{-/-}$ neonatal mouse ventricular cells suspended in mouse media were rotated at 50 rpm on a gyratory shaker (195-mm diameter) for 6–8 h at 37°C and 5% CO_2 to allow aggregation of small, uniform clusters of viable cells. After rotational culture, ~8.0×10^5 CMs were suspended in 83.3 µl of mouse media and added to 116.7 µl of an mECT matrix mixture consisting of 66.7 µl of 2 mg/ml acid-soluble rat tail collagen type I, pH 3.0 (Sigma-Aldrich), 8.3 µl of 10× MEM (Gibco), 8.3 µl of reconstitution buffer (200 mmol/liter $NaHCO_3$, 200 mmol/liter HEPES, and 100 mmol/liter NaOH [Sigma-Aldrich]), and 33.3 µl Matrigel (BD). 200 µl of the cell/matrix suspension was cast into 20 mm × 3 mm cylinder constructs using a Flexcell Tissue Train silicone membrane culture plate (Flexcell International) and incubated under preprogrammed vacuum conditions for 120 min (37°C, 5% CO_2) to form cylindrical-shaped mECT constructs that were attached at each end to fibrin tabs. Upon matrix polymerization, mouse media was added to the mECT within the 6-well culture dish. mECT constructs were maintained in culture for 7 d with media changes every other day.

Mechanical testing of mECT

Isometric force generated by mECT was measured using protocols similar to those previously described (Tobita et al., 2006; de Lange et al., 2011). In brief, each mECT construct was transferred from the culture dish to a model 801B small intact fiber test apparatus (Aurora Scientific) in Krebs-Henseleit buffer (119 mmol/liter NaCl, 12 mmol/liter glucose, 4.6 mmol/liter KCl, 25 mmol/liter $NaHCO_3$, 1.2 mmol/liter KH_2PO_4, 1.2 mmol/liter $MgCl_2$, and 1.8 mmol/liter $CaCl_2$, gassed with 95% O_2/5% CO_2, pH 7.4). mECT constructs were attached with sutures between a model 403A force transducer (Aurora Scientific) and model 322C high-speed length controller (Aurora Scientific). mECTs were perfused with 24°C Krebs-Henseleit buffer at a rate of 1 ml/min, and field stimulation was initiated at 2 Hz (2.5 ms, 8–12.5 V). The longitudinal length of each construct was increased stepwise until maximal twitch force was achieved. mECTs were then equilibrated

for 10–20 min or until a stable level of passive tension was achieved while being paced at 2 Hz. The pacing frequency was increased to 6 Hz, and the temperature of the perfusate in the chamber was adjusted to 37°C before force measurements were made at stimulation frequencies of 6 and 9 Hz. Subsequent to these measurements, mECTs were perfused with 5 µmol/liter dobutamine-containing Krebs-Henseleit buffer before reassessment of contractile function at stimulation frequencies of 6 and 9 Hz. Data from force measurements were analyzed and averaged using IonWizard 6.0 software (IonOptix). For each stimulation frequency, force of 80–160 successive contractions was collected and averaged. Contraction data were exported to Microsoft Excel, and the magnitude and kinetics of force generation were calculated.

Intracellular free Ca^{2+} ion transient measurement

Simultaneous force and Ca^{2+} transient measurements in mECT were performed similar to previously described methods for papillary muscle (Tong et al., 2004). In brief, mECTs were mounted to a force transducer in a perfusion chamber and were loaded for 60 min at room temperature with a Fura-2AM loading solution consisting of Krebs-Henseleit buffer supplemented with 5 µM Fura-2AM (Invitrogen), 1% (vol/vol) Cremophor EL (Sigma-Aldrich), and 10 µmol/l *N,N,N′,N′*-tetrakis(2-pyridylmethyl)ethylene-diamine (Sigma-Aldrich) with constant oxygenation. After loading, mECTs were allowed to recover for 10–20 min at 37°C while being perfused with Krebs-Henseleit buffer with pacing at 4 Hz. Subsequently, Fura-2 fluorescence (a measure of intracellular Ca^{2+}) was measured by alternately illuminating the preparation with 340- and 380-nm light (at a frequency of 250 Hz) through a Plan-Fluor 10× objective on an Eclipse Ti microscope (Nikon). Similarly, emitted light passed through the same Plan-Fluor 10× objective, and 510-nm emission was measured using IonOptix hardware and software with field stimulation at frequencies of 6 and 9 Hz (2.5 ms, 6.5–12.5 V). The emitted fluorescence and force data were stored for offline analysis as the 340- and 380-nm counts. Force generation data were obtained concurrently. The intracellular Ca^{2+} concentration $[Ca^{2+}]_i$ was estimated by the equation: $[Ca^{2+}]_i = K_{Apparent}(R - R_{Min}/R_{Max} - R)$, where R is the ratio of Ca^{2+}-bound Fura-2 fluorescence at 340-nm excitation versus Ca^{2+}-free Fura-2 fluorescence at 380-nm excitation. R_{Min} is measured when Fura-2 is completely free of Ca^{2+}, and R_{Max} is measured when Fura-2 is saturated with Ca^{2+}. $K_{Apparent}$ is the association constant of Fura-2. R_{Min}, R_{Max}, and $K_{Apparent}$ were established empirically on equipment used as these values are influenced by excitation and emission filters, dichroic mirrors, and the microscope objective lens.

Although we do show Ca^{2+} transient magnitude data in Tables S2–S4, these measurements are fraught with difficulty in relatively large multicellular preparations such as mECT in which Ca^{2+} transients are only measured in a small subpopulation of cells. We therefore emphasize the kinetics of the Ca^{2+} transient and the relative effect of interventions such as adrenergic stimulation and increasing frequency within a preparation.

Routine histology and light microscopy

Neonatal and 10-d-old mouse hearts were fixed with Dent's fixative (20% DMSO/80% MeOH) at 4°C overnight. The samples were subsequently transferred to 100% MeOH and stored at −20°C for at least 24 h before being embedded with paraffin using standard protocols. Embedded hearts were then sectioned at a thickness of 8 µm using an RM2165 microtome (Leica), and sections were placed on charged glass microscope slides (Superfrost Plus; Thermo Fisher Scientific) and allowed to dry overnight at 35°C on a flattening plate. Before staining with hematoxylin and eosin (H&E) using SelecTec reagents and protocols (Surgipath), slides were incubated at 68°C for 1 h, submerged twice in xylenes for 2 min each, and rehydrated through EtOH series to water. After staining, sections were coverslipped using Micromount slide-mounting fluid (Surgipath). Sections were visualized and photographed on an Eclipse 90i photomicroscope (Nikon) using a Plan-Fluor 4× objective (Nikon), DS-Fi1 color camera (Nikon), and Elements imaging software (version 4.0; Nikon) and collated using Photoshop (version 12.0.4 x64; Adobe).

Immunohistochemistry

For immunohistochemistry, ECT constructs were rinsed once for 1 min in 0.1 mol/liter KCl to relax the sarcomeres and then once for 1 min in 1× PBS, pH 7.0, before being fixed in Dent's fixative (80% methanol/20% DMSO) for 2 h at 4°C. Constructs were then dehydrated in methanol series and stored at −20°C for 24 h. For sectioning, fixed constructs were transferred directly to xylenes and allowed to equilibrate for 5 min before being placed in paraffin and maintained at 60°C for 90 min. They were subsequently embedded in fresh paraffin in disposable plastic molds and allowed to cool before being sectioned at 8 µm on an RM2165 microtome (Leica), mounted on glass sides, and dried overnight on a flattening plate at 37°C. After drying, slides were heated to 60°C, placed in xylenes for 5 min, rehydrated through ethanol series to water, and rinsed twice in 1× PBS. Blocking was performed in two steps to minimize nonspecific binding of mouse- and goat-derived antibodies. First, slides were blocked for 1 h in 1× PBS containing 5% (vol/vol) sheep serum, 2 mg/ml bovine serum albumin, and 0.1% (vol/vol) Tween 20 and then blocked secondarily with the VECTASTAIN mouse on mouse (M.O.M.) basic kit (Vector Laboratories) according to the manufacturer's instructions. Sections were incubated with 1:100 anti-cMyBPC rabbit polyclonal antibody (Harris et al., 2002) for 1 h at room temperature in M.O.M. protein solution (Vector Laboratories) in a humidity chamber. After rinsing twice for 2 min in PBS, sections were incubated for 1 h at room temperature in the dark with 1:200 Alexa Fluor 647 goat anti–rabbit IgG (H+L) secondary antibody (Molecular Probes) in M.O.M. protein solution as before. After rinsing twice for 2 min in PBS, sections were coverslipped using warmed ProLong Gold Antifade Reagent (Invitrogen) with 4′,6-diamidino-2-phenylindole (DAPI). Imaging was performed using the Eclipse 90i fluorescent confocal microscope using a 40× oil-immersion objective and 405 nm and 647 nm to excite DAPI and Alexa Fluor 647, respectively. Images were acquired using a built-in automated tile scan routine and NIS-Elements software suite.

Echocardiography

1- and 10-d-old WT and $cMyBPC^{-/-}$ mouse pups were used for transthoracic echocardiography using standard protocols. In brief, 10-d-old mice were anaesthetized using inhaled 1% isoflurane, delivered via nose cone, with the flow titrated to minimize bradycardia and maintain a target heart rate of 450 ± 50 beats per minute. Conscious 1-d-old and anesthetized 10-d-old mice were taped in a left lateral decubitus position on a warmed platform, and chest hair was removed with a topical depilatory agent. Hearts were imaged using a Vevo 770 ultrasonograph (Visual Sonics) with a 40-MHz transducer (Agilent Technologies). Two-dimensionally guided M-mode images were acquired at the tip of papillary muscles, and transmitral and aortic velocities were measured using Doppler pulse wave imaging. End diastolic and systolic left ventricular (LV) diameter, as well as anterior and posterior wall (AW and PW, respectively) thickness, was measured on line from M-mode images using the leading edge to leading edge convention. All parameters were measured over at least three consecutive cardiac cycles and averaged. LV mass was calculated by $[1.05 \times ((\text{PW diastole} + \text{AW diastole} + \text{LV diameter diastole})^3 - (\text{LV diameter diastole})^3)]$. LV volume during diastole was calculated by $[(7/(2.4 + \text{LV diameter in diastole})) \times (\text{LV diameter in diastole})^3 \times 1{,}000]$. LV volume during systole was calculated by $[(7/(2.4 + \text{LV diameter in systole})) \times (\text{LV diameter in systole})^3 \times 1{,}000]$. Heart rate was determined from at least three consecutive intervals

from pulse wave Doppler tracings of the LV outflow tract. Ejection fraction was calculated by [100 × ((LV volume diastole − LV volume systole)/LV volume diastole)]. Stroke volume was calculated by [LV volume diastole − LV volume systole]. Cardiac output was calculated by [stroke volume × heart rate]. Isovolumic relaxation time was measured as the time between closing of the aortic value and the opening of the mitral value from pulse wave Doppler tracings of the LV outflow tract and mitral inflow region.

Data and statistical analysis

SPSS software was used to perform statistical analysis. Student's *t* tests were used for two-way comparisons between WT and cMyBP-C$^{-/-}$ mECT or mouse pups. Paired Student's *t* tests were used when comparing pre- and postdobutamine values at each frequency for each mECT. All error bars are SEM. Statistical significance was set at $P < 0.05$. Data from force and intracellular free Ca^{2+} ion transient measurements were analyzed using IonOptix software. For each stimulation frequency, under each condition, force and/or intracellular free Ca^{2+} ion transients of 40–60 successive contractions were collected and averaged. These data were exported to Excel (Microsoft), and the magnitude of force generated and/or Ca^{2+} transients as well as the kinetics of force generation and relaxing and/or Ca^{2+} release and sequestration were calculated.

Online supplemental material

Fig. S1 shows the gross morphological as well as histological structure of mECT used. Fig. S2 shows histological quantification of CM cross-sectional area in WT and cMyBP-C$^{-/-}$ mECTs, showing the lack of CM hypertrophy as a result of cMyBP-C ablation. Detailed data regarding mECT twitch force production and Ca^{2+} transients, depicted in Figs. 2–4, are provided in Tables S1–S4. Online supplemental material is available at http://www.jgp.org/cgi/content/full/jgp.201210837/DC1.

RESULTS

mECTs are derived from prehypertrophic cMyBP-C$^{-/-}$ CMs

To study the primary effects of cMyBP-C ablation on cardiac contraction, it is critical to determine that mECTs are derived from prehypertrophic mouse hearts. We assessed the magnitude of hypertrophic remodeling by routine histology and by measuring heart/body weight ratios at postnatal day 1 and day 10 in WT and cMyBP-C$^{-/-}$ pups. cMyBP-C ablation did not affect gross cardiac morphology at postnatal day 1 (Fig. 1, A and C). By day 10, cMyBP-C$^{-/-}$ hearts were enlarged with pronounced increases in the thickness of the interventricular septum and LV free wall and increased LV chamber diameter (Fig. 1, B and D). Additionally, heart/body weight ratios were similar between neonatal WT and cMyBP-C$^{-/-}$ pups but significantly elevated in 10-d-old cMyBP-C$^{-/-}$ pups (Fig. 1 E). Together, these data suggest that hypertrophic remodeling occurs rapidly during early postnatal development in cMyBP-C mice, but is largely absent at birth, and is supported by previous data that suggests the absence of hypertrophy in neonatal cMyBP-C$^{-/-}$ pups (de Lange et al., 2011).

Hypertrophic remodeling had a profound adverse effect on cardiac function as indicated by the finding that although ejection fraction was similar in nonhypertrophied neonatal cMyBP-C$^{-/-}$ and WT hearts (73.9 ± 4.5% vs. 62.7 ± 4.9%; $P = 0.108$), it was dramatically reduced in cMyBP-C$^{-/-}$ hearts by postnatal day 10 (74.4 ± 5.4% vs. 32.1 ± 3.6%; $P < 0.001$; Fig. 1 F). Notwithstanding the decreased ejection fraction in 10-d-old cMyBP-C$^{-/-}$ mice, the cardiac output (Fig. 1 G) was not affected by cMyBP-C ablation, suggesting that remodeling events between days 1 and 10 are effectively compensatory.

In light of these findings, mECTs used in this study were produced using cardiac cells derived from postnatal day 1 WT and cMyBP-C$^{-/-}$ hearts (Fig. S1). Unlike in the developing cMyBP-C$^{-/-}$ heart that rapidly remodels during the perinatal period, resulting in impaired contractility, cMyBP-C$^{-/-}$ mECTs do not undergo similar hypertrophic remodeling in culture as assessed by CM cross-sectional area (Fig. S2) and equivalent expression levels of the hypertrophic marker genes *Nppa*, *Nppb*, and *MyH7* (de Lange et al., 2011), making mECT a good model system to study the primary effects of cMyBP-C ablation on cardiac contraction.

Accelerated twitch kinetics in cMyBP-C$^{-/-}$ mECT

mECTs generating twitch force between 0.25 and 1 mN were selected to assess the effect of cMyBP-C ablation on cardiac contractile kinetics to minimize possible genotype-dependent contribution of twitch force magnitude to contractile kinetics (WT = 0.556 ± 0.079 mN; cMyBP-C$^{-/-}$ = 0.587 ± 0.065 mN; $n \geq 6$; $P = 0.72$ at 6 Hz). All twitch force and dF/dt (mN/s) traces were plotted as amplitude-normalized curves (normalized to maximum twitch force produced [F_{Max}] for the particular preparation [mN/mN_{FMax} for twitch force and $mN/s/mN_{FMax}$ for dF/dt]) in a similar fashion to other studies (Nagayama et al., 2007; Janssen, 2010).

Overall, contractile kinetics were significantly faster in cMyBP-C$^{-/-}$ than in WT mECT at both frequencies tested (Fig. 2, A and B; and Table S1). In subsequent analysis, twitch timing was divided into four phases (CT_{50} = time to 50% F_{Max}; $CT_{50–100}$ = time 50% F_{Max} to F_{Max}; RT_{50} = F_{Max} to 50% force decay; $RT_{50–90}$ = 50 to 90% force decay). Ablation of cMyBP-C significantly shortened both contractile phases (Fig. 2, C and D) and dramatically shortened the initial phase of relaxation (RT_{50}; Fig. 2 E) at both pacing frequencies. The second phase of relaxation ($RT_{50–90}$) was unaffected by cMyBP-C ablation (Fig. 2 F).

Analysis of the first order derivative (dF/dt) traces in WT and cMyBP-C$^{-/-}$ mECT provided further insight into the contractile effects of cMyBP-C. These data show that both the maximal velocities of contraction ($+dF/dt_{Max}$) and relaxation ($-dF/dt_{Max}$) were higher in cMyBP-C$^{-/-}$ than in WT mECT (Fig. 3, A–D; and Table S1), indicating both faster contractile and relaxation velocities. Interestingly, the $-dF/dt_{Max}/+dF/dt_{Max}$ ratio remained unaffected by cMyBP-C ablation (Fig. 3 E). We subsequently

analyzed the timing of the dF/dt traces and showed that the time to $+dF/dt_{Max}$ was not significantly affected by cMyBP-C ablation (Fig. 3 F). The time from $+dF/dt_{Max}$ to F_{Max} (dF/dt_0) was significantly shorter in cMyBP-C$^{-/-}$ mECT at both pacing frequencies (23.9–26.8%; Fig. 3 G). The most dramatic difference between WT and cMyBP-C$^{-/-}$ mECT was found in the time from F_{Max} to $-dF/dt_{Max.}$ The profound shortening of this interval (40.5–43.6%) in cMyBP-C$^{-/-}$ mECT (Fig. 3 H) corresponds to the significant early drop-off in twitch force as shown in Fig. 2. These data have clear implications for the role of cMyBP-C in influencing actin-myosin cross-bridge attachment–detachment rates and may be the primary contractile defect that triggers compensatory hypertrophic remodeling in the perinatal heart.

cMyBP-C$^{-/-}$ mECTs are unable to accelerate contractile kinetics in response to physiological stimuli

To gain a better understanding of the role that cMyBP-C plays in modulating contractile kinetics in response to lusitropic physiological stimuli, we assessed the effect of increasing pacing frequency and β-adrenergic stimulation in WT and cMyBP-C$^{-/-}$ mECT. Unlike WT mECT, which demonstrated shorter relaxation intervals as pacing frequency increased from 6 to 9 Hz (RT_{50} = −15.0% [P = 0.019] and $RT_{50–90}$ = −27.2% [P < 0.001]), the already accelerated cMyBP-C$^{-/-}$ mECT did not demonstrate significant frequency-dependent acceleration of relaxation (RT_{50} = −4.8% [P = 0.991] and $RT_{50–90}$ = −7.6% [P = 0.903]; Fig. 2, E and F).

Amplitude-normalized averaged twitches, prior and subsequent to dobutamine (β1-aggonist) stimulation,

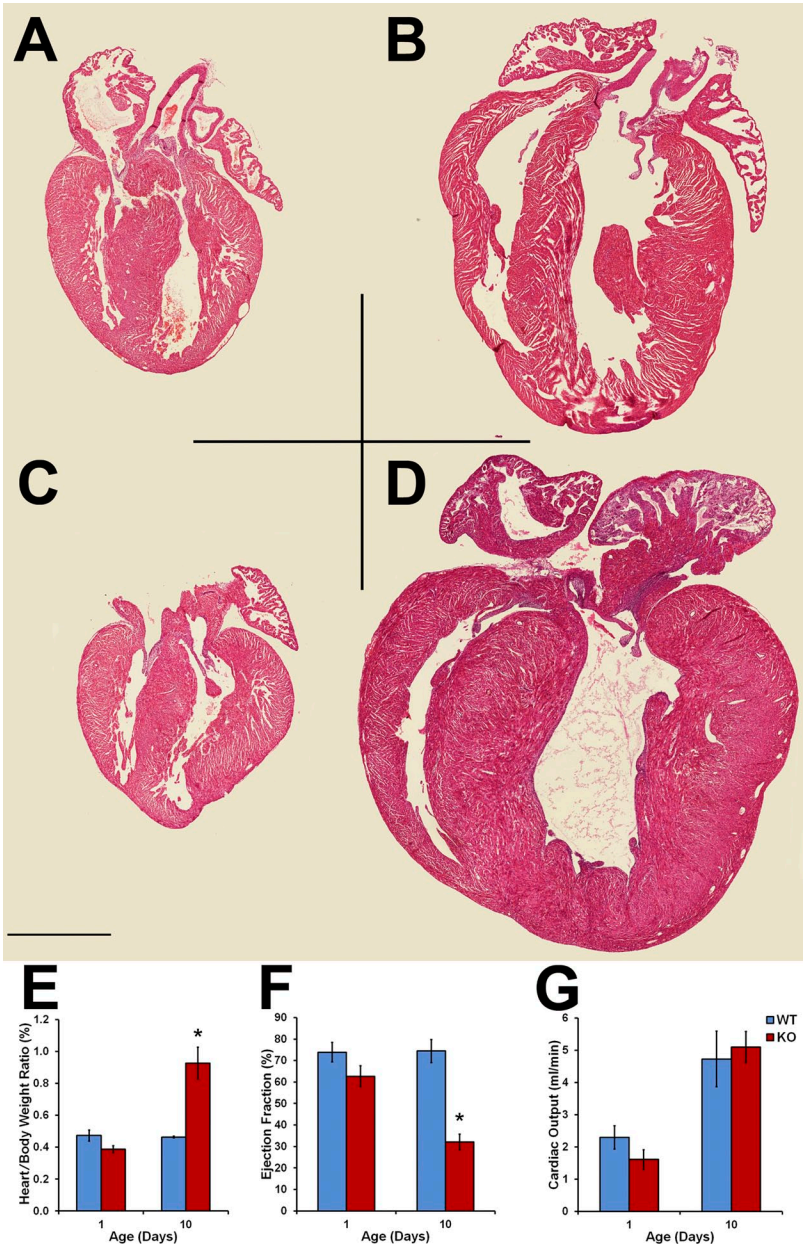

Figure 1. Morphological and functional analyses of neonatal and 10-d-old WT and cMyBP-C$^{-/-}$ hearts. (A–D) H&E-stained thin sections of 1-d-old WT (A), 10-d-old WT (B), 1-d-old cMyBP-C$^{-/-}$ (C), and 10-d-old (D) mouse hearts. Bar, 1 mm. (E–G) Heart/body weight ratios (E), ejection fraction (F), and cardiac output (G) of 1- and 10-d-old WT and cMyBP-C$^{-/-}$ mice are shown. Error bars indicate SEM. *, P < 0.05 versus age-matched WT (Student's *t* test; day 1 WT, *n* = 6; day 1 cMyBP-C$^{-/-}$, *n* = 7; day 10 WT, *n* = 6; day 10 cMyBP-C$^{-/-}$, *n* = 7).

are shown for WT and cMyBP-C$^{-/-}$ (Fig. 2, A and B) mECT. Dobutamine pretreatment had no significant effect on either of our two defined phases of contraction in WT or cMyBP-C$^{-/-}$ mECT (Fig. 2, C and D). As expected, dobutamine treatment significantly shortened RT_{50} in WT mECT (6 Hz = −26.1% [P < 0.001] and 9 Hz = −16.2% [P = 0.041]) but had minimal effect on the constitutively faster cMyBP-C$^{-/-}$ mECT (6 Hz = −6.1% [P < 0.963] and 9 Hz = −7.9% [P = 0.901]; Fig. 2 E). Although dobutamine treatment significantly shortened $RT_{50–90}$ in both WT (−36.8%; P < 0.001) and cMyBP-C$^{-/-}$ (−20.7%; P = 0.023) mECT when paced at 6 Hz, the relative shortening was more striking in the WT group (Fig. 2 F).

Analyses of normalized dF/dt traces prior and subsequent to dobutamine stimulation (Fig. 3) indicate that β1-adrenerdic stimulation does not affect $+dF/dt_{Max}$ in either WT or cMyBP-C$^{-/-}$ mECT (Fig. 3 C). Although dobutamine stimulation increased $-dF/dt_{Max}$ in WT mECT (6 Hz = 53.9% [P < 0.001] and 9 Hz = 23.8% [P = 0.055]), this effect was severely blunted in cMyBP-C$^{-/-}$ mECT (6 Hz = 13.0% [P = 0.310] and 9 Hz = 12.9% [P = 0.299]; Fig. 3 D). Dobutamine stimulation failed to affect the time to $+dF/dt_{Max}$ (Fig. 3 F) and from $+dF/dt_{Max}$ to F_{Max} (Fig. 3 G) at either frequency, independent of genotype. Dobutamine stimulation significantly shortened the time from F_{Max} to $-dF/dt_{Max}$ in WT (6 Hz = −21.3% [P = 0.031] and 9 Hz = −25.3% [P = 0.014]) but did not shorten the same interval in cMyBP-C$^{-/-}$ mECT (6 Hz = −2.3% [P = 1.000] and 9 Hz = 3.7% [P = 1.000]; Fig. 3 H). Collectively, the baseline accelerated relaxation kinetics of cMyBP-C$^{-/-}$ mECT and the marginal further acceleration with either increased pacing frequency or adrenergic stimulation suggest that the cMyBP-C$^{-/-}$ CMs exist in an accelerated state with minimal additional kinetic reserve.

Accelerated twitch kinetics in cMyBP-C$^{-/-}$ mECT are not caused by accelerated Ca^{2+} handling

Because the release and reuptake of Ca^{2+} impact contractile kinetics under normal and pathological conditions, we measured Ca^{2+} transient kinetics in mECT at 6- and 9-Hz pacing frequencies and with the addition of dobutamine (Table S2). The normalized Ca^{2+} transient data demonstrate that there is a shorter interval between peak Ca^{2+} and peak twitch force in the cMyBP-C$^{-/-}$ mECT compared with WT (Fig. 4 A). This difference is caused by the accelerated twitch force kinetics because

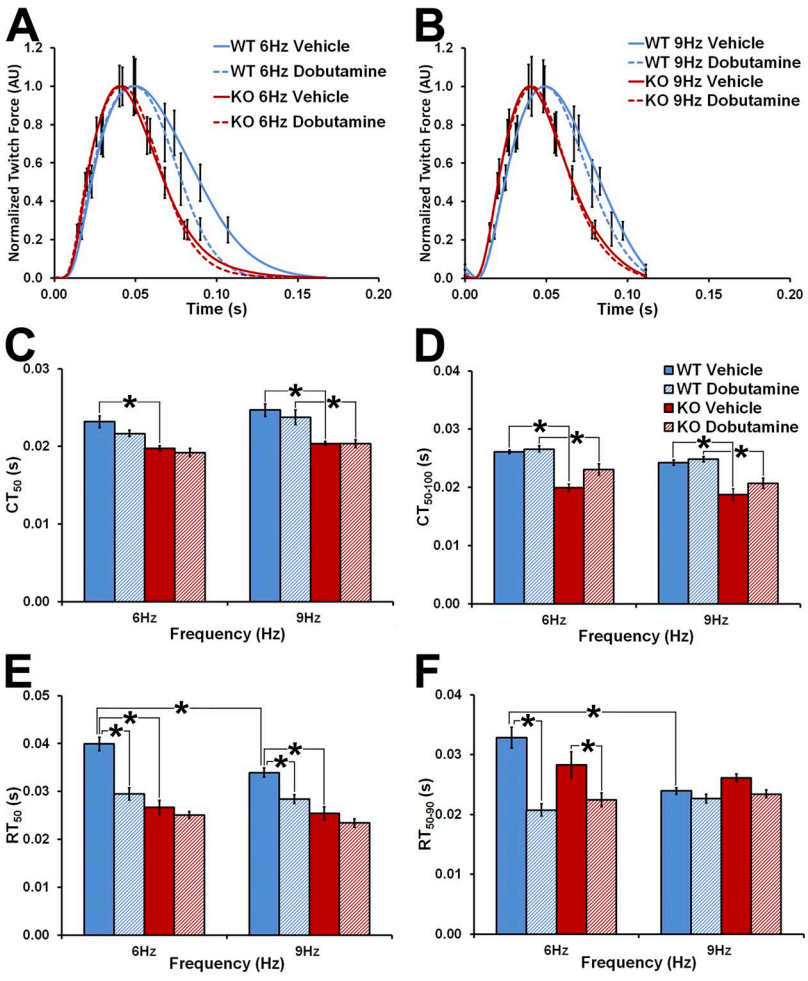

Figure 2. Effect of cMyBP-C ablation on mECT contractile intervals. (A and B) Averaged amplitude-normalized twitch traces of WT and cMyBP-C$^{-/-}$ mECT paced at 6 (A) and 9 Hz (B). Solid blue lines show vehicle-treated WT mECT, solid red lines show vehicle-treated cMyBP-C$^{-/-}$ mECT, dashed blue lines show dobutamine-treated WT mECT, and dashed red lines show dobutamine-treated cMyBP-C$^{-/-}$ mECT. AU, arbitrary units. (C and D) Contraction times from electrical stimulus to 50% of F_{Max} (CT_{50}; C) and from 50% F_{Max} to F_{Max} ($CT_{50–100}$; D) are shown. (E and F) Relaxation times from F_{Max} to 50% twitch force decay (RT_{50}; E) and 50 to 90% twitch force decay ($RT_{50–90}$; F) are shown. (C–F) Blue closed bars show vehicle-treated WT mECT, red closed bars show vehicle-treated cMyBP-C$^{-/-}$ mECT, blue striped bars show dobutamine-treated WT mECT, and red striped bars show dobutamine-treated cMyBP-C$^{-/-}$ mECT. *, P < 0.05 (one-way ANOVA with Tukey's post hoc test; WT, $n = 6$; cMyBP-C$^{-/-}$, $n = 7$). (A–F) Error bars indicate SEM.

there are no differences in the Ca^{2+} transient kinetics between cMyBP-$C^{-/-}$ and WT mECT (Fig. 4 A). Dobutamine stimulation increased the magnitude of the Ca^{2+} transient in a similar fashion in both cMyBP-$C^{-/-}$ and WT mECT (Fig. 4 B), indicating intact adrenergic signaling. The magnitude by which Ca^{2+} transient increased in response to adrenergic stimulation was smaller than those previously observed in adult CMs (Kuznetsov et al., 1995; Peng et al., 2007) but similar to that observed in neonatal CMs (Kuznetsov et al., 1995). This apparent discrepancy is most likely the result of the relative maturity of CMs used to construct mECT, as they are less reliant on intracellular (SR) Ca^{2+} exchange than adult CMs (Escobar et al., 2004).

Increasing pacing frequency did not affect the time to peak Ca^{2+} transient but did accelerate the reuptake of Ca^{2+} as reflected in the more rapid decrease in the transient, independent of mECT genotype (Fig. 4 C). These data indicate that acceleration of twitch force caused by cMyBP-C ablation is likely to result in differences in actomyosin cross-bridge kinetics, rather than changes in Ca^{2+} transient kinetics.

DISCUSSION

mECT as a model of prehypertrophic cMyBP-C HCM

Much of the published work pertaining to the impact of cMyBP-C on cardiac function has relied on mouse

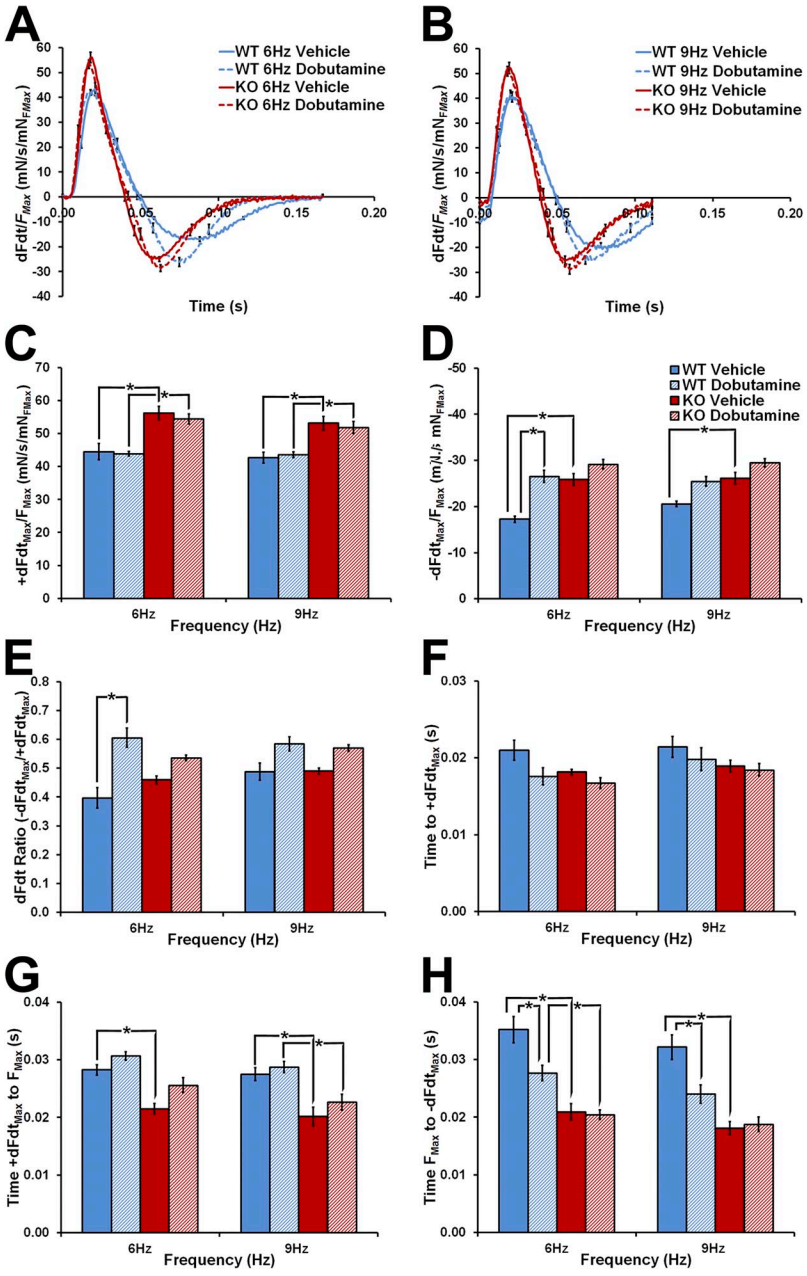

Figure 3. Kinetic effects of cMyBP-C ablation in mECT. (A and B) Averaged amplitude-normalized first order derivative (dF/dt) traces. Solid blue lines show vehicle-treated WT mECT, solid red lines show vehicle-treated cMyBP-$C^{-/-}$ mECT, dashed blue lines show dobutamine-treated WT mECT, and dashed red lines show dobutamine-treated cMyBP-$C^{-/-}$ mECT. (C–E) Normalized maximum contractile velocity ($+dF/dt_{Max}/F_{Max}$; C), normalized maximum relaxation velocity ($-dF/dt_{Max}/F_{Max}$; D), and the dF/dt ratio ($+dF/dt_{Max}/-dF/dt_{Max}$; E). (F–H) The times to $+dF/dt_{Max}$ (F), from dF/dt_{Max} to F_{Max} (G), and from F_{Max} to $-dF/dt_{Max}$ (H). (C–H) Blue closed bars show vehicle-treated WT mECT, red closed bars show vehicle-treated cMyBP-$C^{-/-}$ mECT, blue striped bars show dobutamine-treated WT mECT, and red striped bars show dobutamine-treated cMyBP-$C^{-/-}$ mECT. *, $P < 0.05$ (one-way ANOVA with Tukey's post hoc test; WT, $n = 6$; cMyBP-$C^{-/-}$, $n = 7$). (A–H) Error bars indicate SEM.

models in which significant cardiac remodeling has already occurred. Our objective was to understand the impact of cMyBP-C ablation on contractility without the confounder of hypertrophic remodeling events. In this study, we therefore examined the effects of germline ablation of cMyBP-C on contractile performance in a neonatal engineered multicellular cardiac tissue under near-physiological conditions. Importantly, mECTs were generated from newborn mouse myocardial cells that had yet to undergo the hypertrophic remodeling characteristic of older cMyBP-C$^{-/-}$ mice and in which contractile function was maintained (Harris et al., 2002; de Lange et al., 2011), thereby mitigating the influences of altered cytoarchitecture, Ca^{2+} handling, and energy balance associated with cardiac hypertrophy. Furthermore, establishment of cells in a 3-D integrated environment with cell to cell connections and in the presence of nonmyocytes established a more physiological biomechanical environment than is possible in 2-D cultured cells or traditional skinned fiber preparations.

cMyBP-C as a regulator of cardiac contractility

The current understanding of the regulatory role of cMyBP-C indicates that during low-demand conditions and baseline phosphorylation of cMyBP-C, the inhibitory interaction between cMyBP-C and the S2 domain of myosin results in a smaller proportion of myosin heads being in close proximity to the thin filament, thereby reducing the probability of actomyosin cross-bridge formation (Hofmann et al., 1991; Colson et al., 2008, 2010). When cMyBP-C is either maximally phosphorylated or completely removed, the unrestrained myosin heads move into closer proximity to the thin filament and are more likely to form cross-bridges (Fig. 5; Hofmann et al., 1991; Colson et al., 2008, 2010, 2012). The closer proximity of myosin heads to potential actin-binding sites decreases the time required to propagate cooperative recruitment of cross-bridges and accelerates the rate of force development after Ca^{2+} release (Stelzer et al., 2006b; Moss and Fitzsimons, 2010). This model is supported by several studies that show accelerated contractile kinetics after cMyBP-C ablation (Harris et al., 2002; Korte et al., 2003; Stelzer et al., 2006a,b,c, 2007; Tong et al., 2008) but is refuted by others that showed a deceleration (Carrier et al., 2004; Pohlmann et al., 2007). However, it should be noted that these studies were all performed on adult cMyBP-C$^{-/-}$ mouse hearts that had undergone secondary hypertrophic remodeling and that several were performed on skinned fibers where excitation-contraction coupling was disrupted.

In coupled, nonhypertrophied cMyBP-C$^{-/-}$ mECT, contractile kinetics were significantly accelerated as indicated by increases in $+dF/dt_{Max}$ and $-dF/dt_{Max}$ as well as abbreviation of the CT_{50}, $CT_{50–100}$, RT_{50}, $+dF/dt_{Max}$ to F_{Max}, and F_{Max} to $-dF/dt_{Max}$ intervals. Changes in these contractile kinetic parameters were independent from changes in Ca^{2+} transient kinetics, suggesting that cMyBP-C modulates contractile kinetics at the level of cross-bridge cycling. Thus, removal of the cMyBP-C–imposed constraint on cross-bridge formation, by either ablation or PKA-mediated phosphorylation (Razumova et al., 2006; Tong et al., 2008; Shaffer et al., 2009), positions myosin heads in close proximity to the thin filament (Colson et al., 2007, 2008), resulting in faster cooperative cross-bridge recruitment which in turn leads to faster cross-bridge attachment rates and an acceleration in the rate of contraction.

However, how positioning of the myosin heads close to the thin filament accelerates kinetics during the relaxation phase of the twitch (increased $-dF/dt_{Max}$ and abbreviation of the RT_{50} and F_{Max} to $-dF/dt_{Max}$ intervals) is less intuitive. It was previously shown that physiological manipulations that alter the kinetics of the contraction phase of the twitch were equally reflected during the relaxation phase (Janssen, 2010). In agreement with this concept, we show that although $+dF/dt_{Max}$

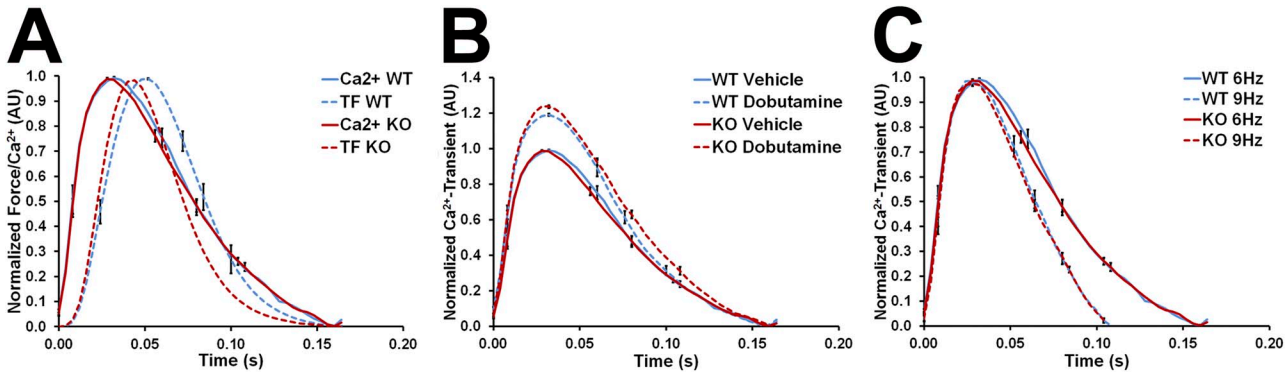

Figure 4. Ca^{2+} transient kinetics in WT and cMyBP-C$^{-/-}$ mECT. (A) Amplitude-normalized twitch force (TF; dashed lines) and Ca^{2+} transient (solid lines) in WT and cMyBP-C$^{-/-}$ mECT paced at 6 Hz. (B) Amplitude-normalized Ca^{2+} transients in vehicle (solid lines)- and dobutamine-treated (dashed lines) WT and cMyBP-C$^{-/-}$ mECT paced at 6 Hz. (C) Amplitude-normalized Ca^{2+} transients in WT and cMyBP-C$^{-/-}$ mECT paced at 6 (solid lines) and 9 Hz (dashed lines). Blue lines (solid and dashed) show WT mECT, and red lines (solid and dashed) show cMyBP-C$^{-/-}$ mECT. (A–C) Error bars indicate SEM. AU, arbitrary units.

and $-dF/dt_{Max}$ were both increased by cMyBP-C ablation, the dF/dt ratio remains unaltered. Furthermore, the notion of accelerated cross-bridge detachment is supported by previous studies that showed cMyBP-C slowing overall actomyosin ATPase rates is likely as the result of slower ATP-induced cross-bridge dissociation (Razumova et al., 2006; Coulton and Stelzer, 2012). The increase in the rate of cross-bridge attachment and force development in cMyBP-$C^{-/-}$ mECT, with a concurrent increase in the rate of cross-bridge detachment, might explain our observed shorter time to F_{Max} with a shortened interval between the unaltered Ca^{2+} transient peak and F_{Max}.

cMyBP-C is essential to the lusitropic response to physiological stimuli

Stimulation of WT mECT with dobutamine significantly and predominantly accelerated the kinetics of the relaxation phase of the twitch, as indicated by a shortening of RT_{50}, $RT_{50–90}$, and F_{Max} to $–dF/dt_{Max}$ intervals and an increase in $-dF/dT_{Max}$. These data correspond to the known positive lusitropic effects of β-adrenergic stimulation (Taffet et al., 1996; Janssen, 2010). When compared with WT mECT, dobutamine stimulation of cMyBP-$C^{-/-}$ mECT uncovered two distinct phases of the relaxation interval: an early phase (as measured by RT_{50} and F_{Max} to $-dF/dt_{Max}$ intervals and increased $-dF/dT_{Max}$) that is cMyBP-C influenced and a late phase ($RT_{50–90}$) that is less influenced by cMyBP-C phosphorylation. Early relaxation velocity is determined by multiple factors including Ca^{2+} reuptake kinetics (Bers and Bridge, 1989) and actin-myosin cross-bridge detachment rates (Razumova et al., 2006; Coulton and Stelzer, 2012). Because we found no differences in the Ca^{2+} transient kinetics between WT and cMyBP-$C^{-/-}$ mECT, we conclude that the observed accelerated early relaxation phase in cMyBP-$C^{-/-}$ mECT is caused by increased cross-bridge detachment rates. The late phase of relaxation accelerated in the cMyBP-$C^{-/-}$ mECT upon dobutamine exposure, albeit not to the magnitude of the WT mECT. This suggests that although faster cross-bridge dissociation caused by cMyBP-C phosphorylation contributes to the abbreviation of this phase, PKA-mediated phosphorylation of other myofibrilar and Ca^{2+} handling/sensing proteins are also involved. Possible candidates, including phosphorylation of cardiac titin (Yamasaki et al., 2002; Krüger and Linke, 2006), cardiac troponin I, or phospholamban (Robertson et al., 1982; Winegrad, 1984; Kranias et al., 1985; Chandra et al., 1997; Frank et al., 2003; Chen et al., 2010), would be expected to influence this phase of relaxation. Previously, we demonstrated that the expression levels of myofibril components and Ca^{2+} handling genes were similar between the WT and cMyBP-$C^{-/-}$ mECT (de Lange et al., 2011), which when combined with the absence of hypertrophic remodeling in our system supports our conclusion that the observed contractile kinetic changes are a direct result of cMyBP-C ablation.

Similar to dobutamine stimulation, an increase in the pacing frequency from 6 to 9 Hz accelerated the rate of relaxation of WT but not cMyBP-$C^{-/-}$ mECT. This suggests a role for cMyBP-C in the frequency-dependent increased rate of cardiac relaxation that is necessary for the heart to function efficiently at higher rates

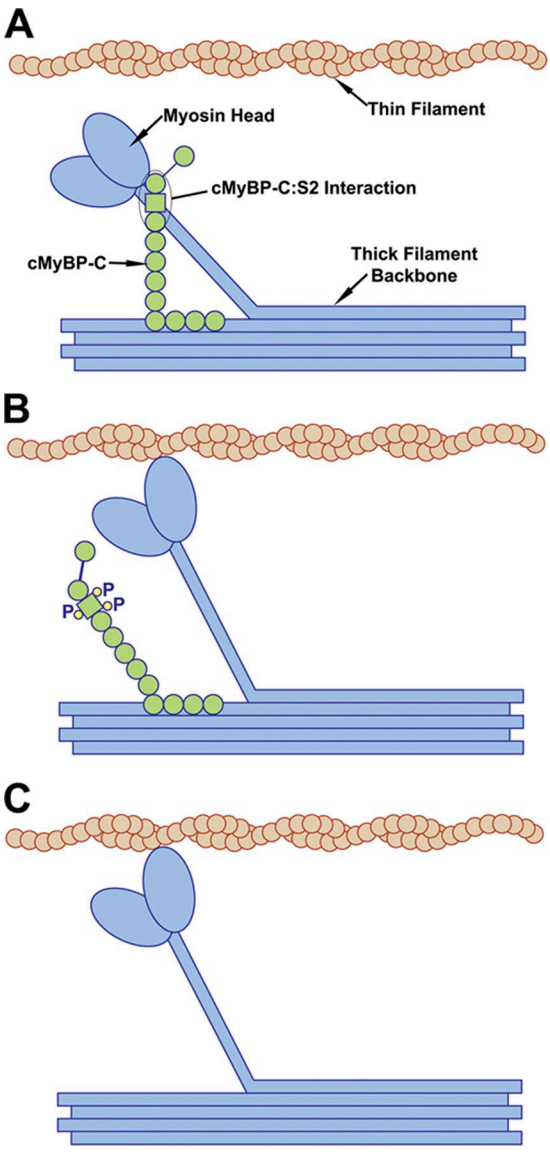

Figure 5. Cartoon showing the proposed effect of cMyBP-C phosphorylation and ablation on myosin head position. (A) Unphosphorylated cMyBP-C interacting with myosin in the S2 coiled-coil, positioning myosin heads further away from the thin filament, thereby decreasing the probability of cross-bridge formation. (B) Maximally phosphorylated cMyBP-C in which interaction with S2 is abolished and myosin heads are positioned closer to the thin filament, thereby increasing the probability of cross-bridge formation. (C) In the absence of cMyBP-C (cMyBP-$C^{-/-}$), myosin heads are positioned closer to the thin filament, thereby increasing the probability of cross-bridge formation. Myosin is shown in blue, actin in tan, and cMyBP-C in green.

(Nagayama et al., 2007; Janssen, 2010). The kinetics of the cMyBP-C$^{-/-}$ twitch is thus revealed to be constitutively accelerated at 6 Hz, with no further acceleration in response to pacing at 9 Hz. This may represent a severe limitation in the dynamic response of the cMyBP-C$^{-/-}$ hearts to increased demand.

Accelerated contractile kinetics as a trigger of hypertrophic remodeling

Hypertrophic and dilatory remodeling of the left ventricle of cMyBP-C$^{-/-}$ mice, while not present at birth, occurs rapidly during the first 10 d of life, as shown in Fig. 1. Similar to previous studies in older animals (Harris et al., 2002; Brickson et al., 2007; Tong et al., 2008), we found that by postnatal day 10, cMyBP-C ablation significantly reduces ejection fraction, whereas function is relatively normal in newborn cMyBP-C$^{-/-}$ hearts. Interestingly, overall cardiac output is similar in 10-d-old WT and cMyBP-C$^{-/-}$ hearts, reflecting the likely effect of increased chamber dimension on preservation of stroke volume. These findings suggest that early compensatory remodeling events effectively maintain stable cardiac output. These data together with the mECT data showing constitutively accelerated contraction kinetics in the absence of activation of hypertrophic signaling suggest that acceleration of contractile kinetics precedes hypertrophic remodeling and may be the trigger for the development of hypertrophy during the perinatal transition. This conclusion is strongly supported by the findings of Chen et al. (2012), who showed accelerated contractile kinetics, manifested as an abbreviated ejection time which preceded remodeling in a cardiac-specific inducible cMyBP-C$^{-/-}$ model.

An important remaining question pertains to how cMyBP-C deficiency, with an intrinsic primary gain of function at the level of the sarcomere, leads to the development of the hypertrophic phenotype. We postulate that the constitutively accelerated cross-bridge cycling in the cMyBP-C$^{-/-}$ sarcomere is perceived by the myocytes and tissue as a persistent state of increased demand. Exactly how this status is perceived and transmitted to trigger the hypertrophic response is unknown but might rely on sensors of ATP turnover and/or mechanical stress within the cell. Energy metabolism, oxidative stress, and cytoskeletal pathways are known to be involved in the development of hypertrophy (Ruwhof and van der Laarse, 2000; Ashrafian et al., 2003; Maulik and Kumar, 2012) and thus represent likely targets for further investigation. Ca^{2+} dysregulation, although not directly implicated in our prehypertrophic model of cMyBP-C ablation, is associated with HCM (Morita et al., 2005) and thought to predispose affected patients to fatal arrhythmias. The cause–effect relationship between the underlying sarcomere protein mutation and perturbations in Ca^{2+} handling needs to be firmly established and the implications studied further.

Conclusion

The principle finding of this study is that contractile kinetics are constitutively accelerated in cMyBP-C$^{-/-}$ mECT. Importantly, the magnitude of further acceleration in response to either dobutamine or increased electrical pacing frequency is significantly decreased in the cMyBP-C$^{-/-}$ mECT, implying that cMyBP-C$^{-/-}$ CMs have minimal additional contractile reserve. Notably, the observed accelerated kinetics are not caused by changes in Ca^{2+} transient kinetics. These observations indicate that modulation of contraction velocity is a primary function of cMyBP-C and not caused by secondary remodeling and further suggest that the alterations in contractile kinetics serve as the primary pathophysiologic trigger for the development of hypertrophy in this model of HCM. Remaining to be determined are the molecular sensors that link the baseline-accelerated sarcomere contractile kinetics to the overall cellular hypertrophic response. Understanding this relationship and the pathways mediating the response should lead to novel approaches to prevent and treat HCM.

We are grateful to Drs. Richard Moss and Michael Wilhelm for critical review of the manuscript, Dr. Timothy Hacker for performing echocardiography, and Mr. Robert Gordon for graphic design assistance.

This work was supported by National Heart, Lung, and Blood Institute grant R01HL107367-01 (to J.C. Ralphe) and Children's Cardiomyopathy Foundation grant 133-PRJ32ZU (to J.C. Ralphe).

Edward N. Pugh Jr. served as editor.

Submitted: 24 May 2012
Accepted: 14 November 2012

REFERENCES

Ashrafian, H., C. Redwood, E. Blair, and H. Watkins. 2003. Hypertrophic cardiomyopathy: a paradigm for myocardial energy depletion. *Trends Genet.* 19:263–268. http://dx.doi.org/10.1016/S0168-9525(03)00081-7

Barefield, D., and S. Sadayappan. 2010. Phosphorylation and function of cardiac myosin binding protein-C in health and disease. *J. Mol. Cell. Cardiol.* 48:866–875. http://dx.doi.org/10.1016/j.yjmcc.2009.11.014

Bers, D.M., and J.H. Bridge. 1989. Relaxation of rabbit ventricular muscle by Na-Ca exchange and sarcoplasmic reticulum calcium pump. Ryanodine and voltage sensitivity. *Circ. Res.* 65:334–342. http://dx.doi.org/10.1161/01.RES.65.2.334

Brickson, S., D.P. Fitzsimons, L. Pereira, T. Hacker, H. Valdivia, and R.L. Moss. 2007. In vivo left ventricular functional capacity is compromised in cMyBP-C null mice. *Am. J. Physiol. Heart Circ. Physiol.* 292:H1747–H1754. http://dx.doi.org/10.1152/ajpheart.01037.2006

Carrier, L., R. Knöll, N. Vignier, D.I. Keller, P. Bausero, B. Prudhon, R. Isnard, M.L. Ambroisine, M. Fiszman, J. Ross Jr., et al. 2004. Asymmetric septal hypertrophy in heterozygous cMyBP-C null mice. *Cardiovasc. Res.* 63:293–304. http://dx.doi.org/10.1016/j.cardiores.2004.04.009

Carrier, L., S. Schlossarek, M.S. Willis, and T. Eschenhagen. 2010. The ubiquitin-proteasome system and nonsense-mediated mRNA decay in hypertrophic cardiomyopathy. *Cardiovasc. Res.* 85:330–338. http://dx.doi.org/10.1093/cvr/cvp247

Chandra, M., W.J. Dong, B.S. Pan, H.C. Cheung, and R.J. Solaro. 1997. Effects of protein kinase A phosphorylation on signaling between cardiac troponin I and the N-terminal domain of cardiac troponin C. *Biochemistry.* 36:13305–13311. http://dx.doi.org/10.1021/bi9710129

Chen, P.P., J.R. Patel, I.N. Rybakova, J.W. Walker, and R.L. Moss. 2010. Protein kinase A–induced myofilament desensitization to Ca^{2+} as a result of phosphorylation of cardiac myosin–binding protein C. *J. Gen. Physiol.* 136:615–627. http://dx.doi.org/10.1085/jgp.201010448

Chen, P.P., J.R. Patel, P.A. Powers, D.P. Fitzsimons, and R.L. Moss. 2012. Dissociation of structural and functional phenotypes in cardiac myosin-binding protein C conditional knockout mice. *Circulation.* 126:1194–1205. http://dx.doi.org/10.1161/CIRCULATIONAHA.111.089219

Colson, B.A., T. Bekyarova, D.P. Fitzsimons, T.C. Irving, and R.L. Moss. 2007. Radial displacement of myosin cross-bridges in mouse myocardium due to ablation of myosin binding protein-C. *J. Mol. Biol.* 367:36–41. http://dx.doi.org/10.1016/j.jmb.2006.12.063

Colson, B.A., T. Bekyarova, M.R. Locher, D.P. Fitzsimons, T.C. Irving, and R.L. Moss. 2008. Protein kinase A-mediated phosphorylation of cMyBP-C increases proximity of myosin heads to actin in resting myocardium. *Circ. Res.* 103:244–251. http://dx.doi.org/10.1161/CIRCRESAHA.108.178996

Colson, B.A., M.R. Locher, T. Bekyarova, J.R. Patel, D.P. Fitzsimons, T.C. Irving, and R.L. Moss. 2010. Differential roles of regulatory light chain and myosin binding protein-C phosphorylations in the modulation of cardiac force development. *J. Physiol.* 588:981–993. http://dx.doi.org/10.1113/jphysiol.2009.183897

Colson, B.A., J.R. Patel, P.P. Chen, T. Bekyarova, M.I. Abdalla, C.W. Tong, D.P. Fitzsimons, T.C. Irving, and R.L. Moss. 2012. Myosin binding protein-C phosphorylation is the principal mediator of protein kinase A effects on thick filament structure in myocardium. *J. Mol. Cell. Cardiol.* 53:609–616. http://dx.doi.org/10.1016/j.yjmcc.2012.07.012

Coulton, A.T., and J.E. Stelzer. 2012. Cardiac myosin binding protein C and its phosphorylation regulate multiple steps in the cross-bridge cycle of muscle contraction. *Biochemistry.* 51:3292–3301. http://dx.doi.org/10.1021/bi300085x

Davis, J., M.V. Westfall, D. Townsend, M. Blankinship, T.J. Herron, G. Guerrero-Serna, W. Wang, E. Devaney, and J.M. Metzger. 2008. Designing heart performance by gene transfer. *Physiol. Rev.* 88:1567–1651. http://dx.doi.org/10.1152/physrev.00039.2007

de Lange, W.J., L.F. Hegge, A.C. Grimes, C.W. Tong, T.M. Brost, R.L. Moss, and J.C. Ralphe. 2011. Neonatal mouse-derived engineered cardiac tissue: a novel model system for studying genetic heart disease. *Circ. Res.* 109:8–19. http://dx.doi.org/10.1161/CIRCRESAHA.111.242354

Escobar, A.L., R. Ribeiro-Costa, C. Villalba-Galea, M.E. Zoghbi, C.G. Pérez, and R. Mejía-Alvarez. 2004. Developmental changes of intracellular Ca2+ transients in beating rat hearts. *Am. J. Physiol. Heart Circ. Physiol.* 286:H971–H978. http://dx.doi.org/10.1152/ajpheart.00308.2003

Frank, K.F., B. Bölck, E. Erdmann, and R.H. Schwinger. 2003. Sarcoplasmic reticulum Ca2+-ATPase modulates cardiac contraction and relaxation. *Cardiovasc. Res.* 57:20–27. http://dx.doi.org/10.1016/S0008-6363(02)00694-6

Gruen, M., and M. Gautel. 1999. Mutations in beta-myosin S2 that cause familial hypertrophic cardiomyopathy (FHC) abolish the interaction with the regulatory domain of myosin-binding protein-C. *J. Mol. Biol.* 286:933–949. http://dx.doi.org/10.1006/jmbi.1998.2522

Gruen, M., H. Prinz, and M. Gautel. 1999. cAPK-phosphorylation controls the interaction of the regulatory domain of cardiac myosin binding protein C with myosin-S2 in an on-off fashion. *FEBS Lett.* 453:254–259. http://dx.doi.org/10.1016/S0014-5793(99)00727-9

Harris, S.P., C.R. Bartley, T.A. Hacker, K.S. McDonald, P.S. Douglas, M.L. Greaser, P.A. Powers, and R.L. Moss. 2002. Hypertrophic cardiomyopathy in cardiac myosin binding protein-C knockout mice. *Circ. Res.* 90:594–601. http://dx.doi.org/10.1161/01.RES.0000012222.70819.64

Harris, S.P., R.G. Lyons, and K.L. Bezold. 2011. In the thick of it: HCM-causing mutations in myosin binding proteins of the thick filament. *Circ. Res.* 108:751–764. http://dx.doi.org/10.1161/CIRCRESAHA.110.231670

Hofmann, P.A., M.L. Greaser, and R.L. Moss. 1991. C-protein limits shortening velocity of rabbit skeletal muscle fibres at low levels of Ca2+ activation. *J. Physiol.* 439:701–715.

Janssen, P.M. 2010. Kinetics of cardiac muscle contraction and relaxation are linked and determined by properties of the cardiac sarcomere. *Am. J. Physiol. Heart Circ. Physiol.* 299:H1092–H1099. http://dx.doi.org/10.1152/ajpheart.00417.2010

Kensler, R.W., J.F. Shaffer, and S.P. Harris. 2011. Binding of the N-terminal fragment C0-C2 of cardiac MyBP-C to cardiac F-actin. *J. Struct. Biol.* 174:44–51. http://dx.doi.org/10.1016/j.jsb.2010.12.003

Korte, F.S., K.S. McDonald, S.P. Harris, and R.L. Moss. 2003. Loaded shortening, power output, and rate of force redevelopment are increased with knockout of cardiac myosin binding protein-C. *Circ. Res.* 93:752–758. http://dx.doi.org/10.1161/01.RES.0000096363.85588.9A

Kranias, E.G., J.L. Garvey, R.D. Srivastava, and R.J. Solaro. 1985. Phosphorylation and functional modifications of sarcoplasmic reticulum and myofibrils in isolated rabbit hearts stimulated with isoprenaline. *Biochem. J.* 226:113–121.

Krüger, M., and W.A. Linke. 2006. Protein kinase-A phosphorylates titin in human heart muscle and reduces myofibrillar passive tension. *J. Muscle Res. Cell Motil.* 27:435–444. http://dx.doi.org/10.1007/s10974-006-9090-5

Kuznetsov, V., E. Pak, R.B. Robinson, and S.F. Steinberg. 1995. β 2-adrenergic receptor actions in neonatal and adult rat ventricular myocytes. *Circ. Res.* 76:40–52. http://dx.doi.org/10.1161/01.RES.76.1.40

Maulik, S.K., and S. Kumar. 2012. Oxidative stress and cardiac hypertrophy: a review. *Toxicol. Mech. Methods.* 22:359–366. http://dx.doi.org/10.3109/15376516.2012.666650

McConnell, B.K., K.A. Jones, D. Fatkin, L.H. Arroyo, R.T. Lee, O. Aristizabal, D.H. Turnbull, D. Georgakopoulos, D. Kass, M. Bond, et al. 1999. Dilated cardiomyopathy in homozygous myosin-binding protein-C mutant mice. *J. Clin. Invest.* 104:1235–1244. (published erratum appears in *J. Clin. Invest.* 1999. 104:1771) http://dx.doi.org/10.1172/JCI7377

Morita, H., J. Seidman, and C.E. Seidman. 2005. Genetic causes of human heart failure. *J. Clin. Invest.* 115:518–526.

Moss, R.L., and D.P. Fitzsimons. 2010. Regulation of contraction in mammalian striated muscles—the plot *thick*-ens. *J. Gen. Physiol.* 136:21–27. http://dx.doi.org/10.1085/jgp.201010471

Nagayama, T., E. Takimoto, S. Sadayappan, J.O. Mudd, J.G. Seidman, J. Robbins, and D.A. Kass. 2007. Control of in vivo left ventricular [correction] contraction/relaxation kinetics by myosin binding protein C: protein kinase A phosphorylation dependent and independent regulation. *Circulation.* 116:2399–2408. http://dx.doi.org/10.1161/CIRCULATIONAHA.107.706523

Peng, J., K. Raddatz, J.D. Molkentin, Y. Wu, S. Labeit, H. Granzier, and M. Gotthardt. 2007. Cardiac hypertrophy and reduced contractility in hearts deficient in the titin kinase region. *Circulation.* 115:743–751. http://dx.doi.org/10.1161/CIRCULATIONAHA.106.645499

Pohlmann, L., I. Kröger, N. Vignier, S. Schlossarek, E. Krämer, C. Coirault, K.R. Sultan, A. El-Armouche, S. Winegrad, T. Eschenhagen,

and L. Carrier. 2007. Cardiac myosin-binding protein C is required for complete relaxation in intact myocytes. *Circ. Res.* 101:928–938. http://dx.doi.org/10.1161/CIRCRESAHA.107.158774

Razumova, M.V., J.F. Shaffer, A.Y. Tu, G.V. Flint, M. Regnier, and S.P. Harris. 2006. Effects of the N-terminal domains of myosin binding protein-C in an in vitro motility assay: Evidence for long-lived cross-bridges. *J. Biol. Chem.* 281:35846–35854. http://dx.doi.org/10.1074/jbc.M606949200

Robertson, S.P., J.D. Johnson, M.J. Holroyde, E.G. Kranias, J.D. Potter, and R.J. Solaro. 1982. The effect of troponin I phosphorylation on the Ca2+-binding properties of the Ca2+-regulatory site of bovine cardiac troponin. *J. Biol. Chem.* 257:260–263.

Ruwhof, C., and A. van der Laarse. 2000. Mechanical stress-induced cardiac hypertrophy: mechanisms and signal transduction pathways. *Cardiovasc. Res.* 47:23–37. http://dx.doi.org/10.1016/S0008-6363(00)00076-6

Sadayappan, S., J. Gulick, H. Osinska, D. Barefield, F. Cuello, M. Avkiran, V.M. Lasko, J.N. Lorenz, M. Maillet, J.L. Martin, et al. 2011. A critical function for Ser-282 in cardiac Myosin binding protein-C phosphorylation and cardiac function. *Circ. Res.* 109:141–150. http://dx.doi.org/10.1161/CIRCRESAHA.111.242560

Shaffer, J.F., R.W. Kensler, and S.P. Harris. 2009. The myosin-binding protein C motif binds to F-actin in a phosphorylation-sensitive manner. *J. Biol. Chem.* 284:12318–12327. http://dx.doi.org/10.1074/jbc.M808850200

Stelzer, J.E., S.B. Dunning, and R.L. Moss. 2006a. Ablation of cardiac myosin-binding protein-C accelerates stretch activation in murine skinned myocardium. *Circ. Res.* 98:1212–1218. http://dx.doi.org/10.1161/01.RES.0000219863.94390.ce

Stelzer, J.E., D.P. Fitzsimons, and R.L. Moss. 2006b. Ablation of myosin-binding protein-C accelerates force development in mouse myocardium. *Biophys. J.* 90:4119–4127. http://dx.doi.org/10.1529/biophysj.105.078147

Stelzer, J.E., J.R. Patel, and R.L. Moss. 2006c. Protein kinase A-mediated acceleration of the stretch activation response in murine skinned myocardium is eliminated by ablation of cMyBP-C. *Circ. Res.* 99:884–890. http://dx.doi.org/10.1161/01.RES.0000245191.34690.66

Stelzer, J.E., J.R. Patel, J.W. Walker, and R.L. Moss. 2007. Differential roles of cardiac myosin-binding protein C and cardiac troponin I in the myofibrillar force responses to protein kinase A phosphorylation. *Circ. Res.* 101:503–511. http://dx.doi.org/10.1161/CIRCRESAHA.107.153650

Taffet, G.E., L.A. Michael, and C.A. Tate. 1996. Exercise training improves lusitropy by isoproterenol in papillary muscles from aged rats. *J. Appl. Physiol.* 81:1488–1494.

Tobita, K., L.J. Liu, A.M. Janczewski, J.P. Tinney, J.M. Nonemaker, S. Augustine, D.B. Stolz, S.G. Shroff, and B.B. Keller. 2006. Engineered early embryonic cardiac tissue retains proliferative and contractile properties of developing embryonic myocardium. *Am. J. Physiol. Heart Circ. Physiol.* 291:H1829–H1837. http://dx.doi.org/10.1152/ajpheart.00205.2006

Tong, C.W., R.D. Gaffin, D.C. Zawieja, and M. Muthuchamy. 2004. Roles of phosphorylation of myosin binding protein-C and troponin I in mouse cardiac muscle twitch dynamics. *J. Physiol.* 558:927–941. http://dx.doi.org/10.1113/jphysiol.2004.062539

Tong, C.W., J.E. Stelzer, M.L. Greaser, P.A. Powers, and R.L. Moss. 2008. Acceleration of crossbridge kinetics by protein kinase A phosphorylation of cardiac myosin binding protein C modulates cardiac function. *Circ. Res.* 103:974–982. http://dx.doi.org/10.1161/CIRCRESAHA.108.177683

van Dijk, S.J., D. Dooijes, C. dos Remedios, M. Michels, J.M. Lamers, S. Winegrad, S. Schlossarek, L. Carrier, F.J. ten Cate, G.J. Stienen, and J. van der Velden. 2009. Cardiac myosin-binding protein C mutations and hypertrophic cardiomyopathy: haploinsufficiency, deranged phosphorylation, and cardiomyocyte dysfunction. *Circulation.* 119:1473–1483. http://dx.doi.org/10.1161/CIRCULATIONAHA.108.838672

Weisberg, A., and S. Winegrad. 1996. Alteration of myosin cross bridges by phosphorylation of myosin-binding protein C in cardiac muscle. *Proc. Natl. Acad. Sci. USA.* 93:8999–9003. http://dx.doi.org/10.1073/pnas.93.17.8999

Winegrad, S. 1984. Regulation of cardiac contractile proteins. Correlations between physiology and biochemistry. *Circ. Res.* 55:565–574. http://dx.doi.org/10.1161/01.RES.55.5.565

Yamasaki, R., Y. Wu, M. McNabb, M. Greaser, S. Labeit, and H. Granzier. 2002. Protein kinase A phosphorylates titin's cardiac-specific N2B domain and reduces passive tension in rat cardiac myocytes. *Circ. Res.* 90:1181–1188. http://dx.doi.org/10.1161/01.RES.0000021115.24712.99